AIChE

Protein Adsorption Kinetics in Charged Agarose Gels: Effect of Agarose Content and Modeling

Emily B. Schirmer and Giorgio Carta
Dept. of Chemical Engineering, University of Virginia, Charlottesville, VA 22904

DOI 10.1002/aic.11668
Published online December 18, 2008 in Wiley InterScience (www.interscience.wiley.com).

The adsorption kinetics of myoglobin in charged gels of varying agarose content have been measured macroscopically, through batch uptake experiments, and microscopically, using light microscopy with gels supported in microfluidics chips. The apparent effective pore diffusivities, determined by fitting either set of rate data to the shrinking core model, were greater than the free solution diffusivity and concentration-dependent. Moreover, the microscopically derived concentration profiles were qualitatively different from the predicted ones. Therefore, a new model taking into account an assumed favorable partitioning of the protein in the pore liquid is proposed to describe the adsorption kinetics. The new model yields effective pore diffusivities that are in approximate agreement with the values determined chromatographically under nonbinding conditions and with hindered diffusion theory. In addition, it predicts concentration profiles in the gel that are consistent with those observed microscopically. The overall increase in mass transfer is attributed to the favorable partitioning of the protein in the pores at low ionic strength, which results in a greater diffusional driving force.
 AIChE J, 55: 331–341, 2009
Keywords: protein adsorption, diffusion, agarose gels, light microscopy, modeling

Introduction

Transport within the stationary phase is typically the controlling band broadening effect in protein ion exchange chromatography.[1] Thus, understanding and modeling protein transport in these materials is a key step in optimizing process performance. Various methods exist to determine protein adsorption kinetics in chromatographic matrices. These include macroscopic measurements, where mass transfer rates are obtained directly,[2,3] and microscopic methods, where the protein concentration profiles in the stationary phase are measured. The latter approaches give not only rates but also information about the mechanism of transport and include confocal laser scanning microscopy (CLSM),[4–10] refractive index based microscopy,[11,12] and light microscopy using chromophoric proteins diffusing in slab-shaped matrices.[13–15] Each of these methods has advantages and disadvantages. CLSM allows measurements in transparent chromatographic beads using fluorescently labeled protein tracers. However, the quantitative interpretation is often complicated by artifacts arising from the different adsorptive behavior of native and fluorescently labeled protein molecules and by fluorescence attenuation effects.[9,16] Refractive index microscopy, as recently introduced,[11,12] allows measurements with unlabeled proteins but is restricted to cases where the concentration profile is very sharp. Finally, light microscopy with gels supported in square capillaries can provide quantitative insight, but requires special syntheses and is cumbersome when the gel is produced through a multistep process, such as is the case for charged agarose gels.

Recently, we have introduced a light microscopy method to visualize the evolution of protein concentration profiles

Correspondence concerning this article should be addressed to G. Carta at gc@virginia.edu.
Current address for E. B. Schirmer: Percivia LLC, 1 Hampshire Street 5th floor, Cambridge, MA 02139.

using charged agarose gels supported in microfluidics chips.[17] This method offers advantages over CLSM because the proteins do not need to be fluorescently labeled and diffusion can be modeled as a semi-infinite slab. Moreover, the microfluidics format allows for better control of hydrodynamic conditions and permits multiple gel synthesis steps (gel formation, crosslinking, and functionalization) to be conducted on-chip.

In our previous work,[17] we reported experimental results for the three proteins cytochrome-c, myoglobin, and hemoglobin in a 6% agarose-based sulfopropyl-functionalized gel. For all three, adsorption rates obtained from the microscopic experiments were consistent with those observed macroscopically for particles suspended in an agitated contactor. The total amount of protein adsorbed could be described as a function of time by the classical shrinking core model.[18] However, the corresponding apparent effective pore diffusivities, obtained by fitting the model to the rate data, were in most cases higher than in free solution and exhibited a significant dependence on protein concentration. This result is not expected for ordinary diffusion in a porous network, suggesting that a more complex transport mechanism takes place. Moreover, the shell-progressive model was in qualitative disagreement with the experimental concentration profiles as a function of distance. The profiles for cytochrome-c were smooth, despite the highly favorable adsorption isotherm, and qualitatively consistent with surface or a solid-phase diffusion mechanisms. On the other hand, the myoglobin profiles showed a more complex behavior with a smooth portion followed by a sharp front, which is not consistent with available models.

The objective of this article is thus threefold. The first is to extend our measurements of adsorption kinetics to gels with different agarose contents. The second is to determine effective pore diffusivities from isocratic elution experiments under non-retained conditions, i.e., where attractive protein-surface interactions are absent. The third objective is to develop a conceptual model to describe the myoglobin adsorption kinetics.

Materials and Methods

Materials

Materials used for this work were as described in our previous article.[17] Briefly, agarose gels were synthesized with high gel strength agarose from USB Corporation (Cleveland, OH), crosslinked with epichlorohydrin (EPC), allylated with allyl glycidyl ether (AGE), and converted to sulfopropyl (SP) cation exchangers by reaction of the allyl groups with sodium metabisulfite. All chemicals used in these steps were from Sigma Chemical Co. (St. Louis, MO) and Fisher Scientific (Fair Lawn, NJ). Borofloat® glass slides spin-coated with chrome and photoresist coatings used to prepare the microfuidics chips were from Nanofilms (West Lake, CA).

Dextran standards (T fractions) used in inverse size exclusion chromatography (iSEC) and myoglobin (horse, M_r = 17 kDa, pI 7.2) were from GE Healthcare (Piscataway, NJ) and Sigma (St. Louis, MO), respectively. All experiments were conducted in 20 mM sodium acetate adjusted to pH 5.0 with acetic acid. These conditions (about 2 pH units away from the protein pI and low ionic strength) were chosen to give favorable binding of myoglobin.

Table 1. Materials Properties*

Agarose Content	4%	6%	9%
q_0† (μmol/cm^3)	120	150	305
ρ_{pw}‡ (g wet/cm^3)	1.02	1.03	1.06
ρ_d§ (g dry/cm^3)	0.07	0.10	0.16
ε_p¶	0.90	0.83	0.69
$\bar{r}_{pore}^{(e)}$** (nm)	18.5	6.4	2.8
$\bar{r}_p^{(f)}$† (μm)	50	64	91

*The 6% data are from Schirmer and Carta.[17]
†Total ionic capacity determined by titration.
‡Hydrated particle density determined picnometrically.
§Dry particle density determined from weight loss at 110°C.
¶ε_p, Total porosity determined from chromatographic retention of glucose.
**$\bar{r}_{pore}$, average pore radius determined from iSEC.
$\bar{r}_p$, volume-average particle radius.

Methods

Agarose gels were prepared and functionalized as previously described[17] either by casting into the microfluidics chips to form 100 μm-thick slabs for microscopic visualization experiments or emulsifying in cyclohexane with 2% (w/v) SPAN 85 to form spherical beads.

Three different agarose concentrations were used: 4, 6, and 9% (w/v), all based on the agarose content of the starting solutions. Ionic capacity, particle density, particle size distribution, porosity, and pore size were determined as previously described and are summarized in Table 1. The pore radii were determined by iSEC with dextran probes (5, 10, 25, 40, 70, and 500 kDa), based on a cylindrical pore model assuming a uniform pore size distribution using the procedure described in detailed in Ref. 17. Although a pore size distribution could in principle be obtained, as is typically found,[19] the iSEC results did not permit a unique determination since many different distributions provided an equally good fit of the data. Thus, we just chose the simplest model assuming a uniform pore size. The retention of glucose was used to calculate the intraparticle porosity. As expected, as the agarose content increases, the bead density and the ionic capacity increase but the pore size and porosity decrease.

Protein adsorption isotherms and batch uptake rates, obtained by material balance and protein concentration profiles in the gels, obtained microscopically, were determined as previously described.[17] Briefly, the adsorption isotherms were obtained by suspending small resin samples in protein solutions with different initial concentrations and mixing for 8 h. Based on the kinetic measurements, this time was estimated to be sufficient to attain equilibrium even with the slowest resin considered (see Experimental Results section). For the batch uptake rates, the agarose particles were suspended in a protein solution in an agitated vessel and the amount adsorbed was obtained from the residual protein concentration at each time. For the microscopic determination of protein concentration profiles, the gels were cast into a 100 μm deep, 5 mm long, 1-mm-wide channel etched perpendicular to a flow channel on a glass chip. After functionalization, a glass slide with two holes drilled at positions corresponding with the flow channel was used to seal the assembly. Adsorption experiments were performed by pumping a protein solution through the flow channel and across the exposed edge of the gel and monitoring the evolution of the myoglobin

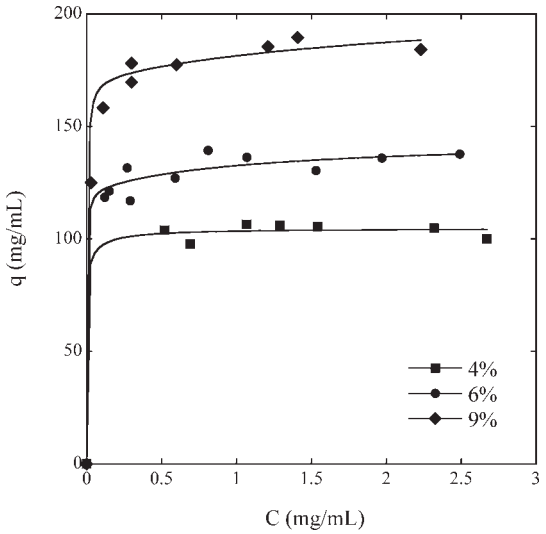

Figure 1. Adsorption isotherms for myoglobin on gels with different agarose content.

Lines are based on Eq. 2 with parameters from Table 2. The 6% data are from Schirmer and Carta.[17]

concentration profiles in the gel with a microscope and CCD camera at 100× magnification. The images were then digitized and the myoglobin concentration profiles obtained from the corresponding smoothed gray-scale intensity with a calibration curve as previously described.[17]

Finally, isocratic elution experiments for unretained conditions were conducted using an AKTA Explorer chromatographic workstation with the functionalized agarose beads packed in 5 mm-diameter Tricorn columns from GE Healthcare. The columns were operated at 0.1–1.5 cm^3/min with 20 μl injections of 2 mg/cm^3 myoglobin. The mobile phase was 20 mM sodium acetate containing 500 mM NaCl at pH 5.0. For these conditions there was no retention of myoglobin as demonstrated by the fact that the myoglobin elution time was consistent with the elution time of dextran with corresponding viscosity radius. The apparent effective pore diffusivity, $D_{e,app}$, was determined for these conditions from the slope of van Deemter curves obtained from the moment method using the following equation[20]

$$\frac{D_{e,app}}{D_0} = \frac{1}{30}\frac{\varepsilon}{1-\varepsilon}\left(\frac{k'}{1+k'}\right)^2\left(\frac{dh}{dv'}\right)^{-1} \quad (1)$$

where D_0 is the free solution diffusivity, ε is the extraparticle porosity, k' is the retention factor, $h = HETP/\bar{d}_p$ is the reduced height equivalent to a theoretical plate (HETP), and $v' = v\bar{d}_p/D_0$ is the reduced velocity. The solution diffusivity $D_0 = 1.1 \times 10^{-6}$ cm^2/s was obtained from Tyn and Gusek,[21] whereas the volume-average particle diameter, $\bar{d}_p$, was calculated from the experimental particle size distributions. ε was obtained from the retention of blue dextran. As for these conditions there is no binding and the protein merely diffuses in the pores, the D_e-value determined from these experiments is expected to represent the true effective pore diffusivity.

Results

Experimental

The adsorption isotherms are shown in Figure 1 for gels with different agarose concentrations. The adsorption capacity increases with agarose concentration as a result of the higher charge density and surface area of the matrix. In each case, the isotherm is highly favorable at low protein concentration, but exhibits a gradual positive slope at higher concentrations. Thus, a heterogeneous bi-Langmuir isotherm[1] was used to fit the data according to the following equation:

$$q = q_a + q_p = \frac{q_{a,m}K_aC}{1+K_aC} + \frac{q_{p,m}K_pC}{1+K_pC} \quad (2)$$

Fitted lines and parameters are shown in Figure 1 and Table 2, respectively. As seen in Figure 1, the fit is within the scatter of the data. From the physical viewpoint, the reasons for this behavior are not precisely known. However, a possibility is that protein is present in the agarose gel either adsorbed on two different sites, one with high affinity and the other with low affinity, or in two different conformations, one strongly and the other weakly bound. In either case, q_a and q_p represent the concentrations of protein molecules held in two different ways within the charged agarose gel.

Batch uptake curves are shown in Figure 2 for a 2 mg/cm^3 initial protein concentration and for gels with different agarose content. To facilitate the comparison, the time scale is normalized by the square of the average particle radius, $\bar{r}_p$, thereby taking into account the different sizes of the three materials. The lines shown were obtained by fitting the shrinking core model taking into account the particle size distribution.[22] The film mass transfer coefficient was estimated based on a Sherwood number ($Sh = k_f\bar{d}_p/D_0$) of 28 and the apparent effective diffusivity, $D_{e,app}$, was determined by matching experimental and calculated uptake curves as in our previous work.[17] A summary of the fitted values normalized by the free solution diffusivity is given in Table 3. As seen from these results, the apparent effective diffusivities are concentration dependent and, with the exception of the 9% agarose matrix, higher than the free solution diffusivity. This result is not expected for ordinary diffusion in agarose gels.[23] The $D_{e,app}$-values can also be used to assess whether equilibrium was established in the isotherm experiments. Based on the shrinking core model,[22] the time needed to attain equilibrium can be estimated as $t^* = q_m r_p^2/6C_0D_{e,app}$. Thus, for 9% agarose and 0.5 mg/cm^3 initial protein concentration, using the $D_{e,app}$ determined at 2 mg/cm^3, we obtain $t^* \sim 4.2$ h, which is considerably less than the 8 h used experimentally. In practice, we observed that $D_{e,app}$ increases as the protein concentration is reduced making the time sufficient even at lower protein concentrations.

Table 2. Adsorption Isotherm Parameters

Agarose Content	4%	6%	9%
$q_{a,m}$ (mg/ cm^3)	92	122	172
K_a (cm^3/mg)	700	500	300
$q_{p,m}$ (mg/ cm^3)	13.8	22.8	36.6
K_p (cm^3/mg)	5.0	0.908	0.376

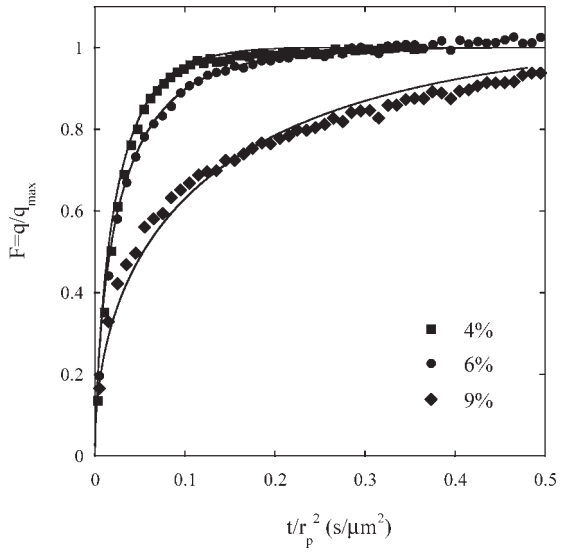

Figure 2. Batch uptake curves for myoglobin on gels with different agarose content for 2 mg/cm^3 initial protein concentration.

The time scale is normalized by the average particle diameter. Lines are based on the shrinking core model with apparent effective diffusivities from Table 3. The 6% data are from Schirmer and Carta.[17]

Concentration profiles obtained microscopically for adsorption in the agarose slabs for conditions analogous to those in Figure 2 are shown in Figure 3. The corresponding microscopically derived uptake curves, $\overline{q}/q_{\max}$ vs. time, obtained by integrating the experimental concentration profiles are shown in Figure 4. The lines in this figure are based again on the shrinking core model, which in this case is given by[18]:

$$\frac{tD_{e,app}}{\ell^2} = \frac{q_{\max}}{C_0}\left[\frac{1}{2}\left(\frac{\overline{q}}{q_{\max}}\right)^2 + \frac{1}{Bi}\left(\frac{\overline{q}}{q_{\max}}\right)\right] \tag{3}$$

where $Bi = k_f\ell/D_{e,app}$ is the Biot number, k_f is the boundary layer mass transfer coefficient, and ℓ is the length of the slab (0.1 cm in our case). The mass transfer coefficient $k_f = 3.4 \times 10^{-4}$ cm/s was as previously determined.[17] As seen in Figure 4, the shrinking core model provides a good description of the slab uptake rate data, although, only of the average $\overline{q}/q_{\max}$ vs. time curves. The corresponding $D_{e,app}$-values are in reasonable agreement with those derived from the macroscopic batch uptake rates but the corresponding concentration profiles in the gel are in disagreement with the experimental ones.

The final set of experimental results is the pulse response experiments shown in Figure 5. Retention decreases as the agarose content increases because of the smaller porosity. In each case, the peaks broaden as the flow rate is increased. For the 9% agarose, in particular, the peaks become highly skewed, despite the lower flow rates used for this material. The corresponding van Deemter curves are linear, as seen in Figure 6, indicating that mass transfer is controlling and exhibit a larger slope at the higher agarose contents. Accordingly, based on Eq. 1, the effective diffusivities are lower. These values are summarized in Table 3 normalized again by the free solution diffusivity and are much smaller than those determined from the adsorption experiments. In this case, the ratio $D_{e,app}/D_0$ is substantially less than unity as expected for ordinary diffusion in the relatively dense agarose matrices used in this work.

Modeling

As shown earlier, the shrinking core model provides a practically useful description of the time course of adsorption, whether in particles suspended in a mixed batch system or in a slab. However, the model obviously fails on physical grounds because of three reasons: (i) the fitted apparent effective diffusivities are larger than the free solution diffusivity and are dependent on the protein concentration to a significant extent. Such behavior is not expected for macropore diffusion because the protein concentration is quite low. (ii) The concentration profiles determined microscopically are different from those predicted for pore diffusion. As the isotherm is very favorable, pore diffusion predicts a simple sharp profile, whereas those seen experimentally exhibit a gradual slope followed by a sharp front. (iii) The fitted diffusivity values under strong binding conditions are very different from those determined from pulse response experiments where interactions between the protein and the stationary phase are presumably purely steric. A possible explanation of these effects is electostatic coupling of diffusion fluxes.[8] However, while electrostatic interactions are obviously a strong contribution to binding at the low ionic strength used in these experiments, although the net charge of myoglobin

Table 3. Summary of Apparent Effective Diffusivity Values Normalized by the Free Solution Diffusivity, $D_{e,app}/D_0$

Conditions		Shrinking Core Model*		Partitioning Model†		Pore Diffusion Model‡
Agarose Content	C_0 (mg/cm^3)	Batch Ads.	Slab Ads.	Batch Ads.	Slab Ads.	Pulse Response
4%	2.0	1.9	2.7	0.27	0.34	0.34
6%	0.5	2.1	2.2	0.16	0.09	
	1.0	1.8	1.6	0.13	0.12	
	2.0	1.5	1.0	0.14	0.12	
	3.0	1.2	0.91	0.18	0.17	
	Avg.	1.6 ± 0.3	1.1 ± 0.3	0.15 ± 0.02	0.13 ± 0.03	0.14
9%	2.0	0.31	0.33	0.032	0.040	0.033

*Based on shrinking core model fit to batch and microscopic adsorption rate data.
†Based on partitioning model fit to batch and microscopic adsorption rate data.
‡Based on chromatographic pulse response for non-binding conditions.

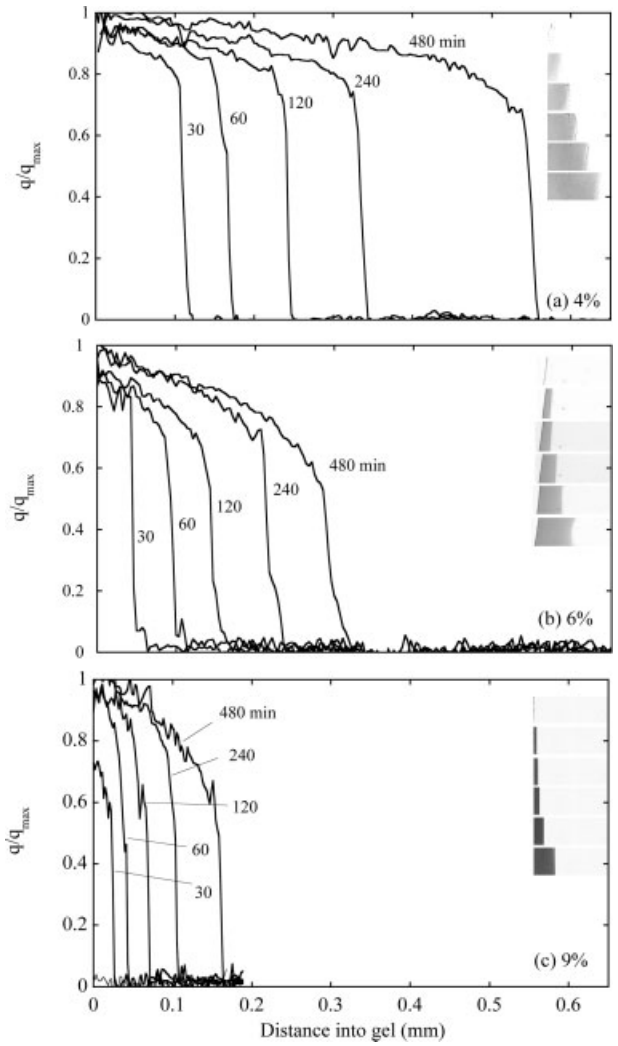

Figure 3. Concentration profiles of 2 mg/cm^3 myoglobin adsorbed in gels with different agarose contents.

Insets show the corresponding digitized gray-scale images. (a) 4%, (b) 6%, and (c) 9% agarose.

is around 12.5 at pH 5, even at 3 mg/cm^3, the protein ionic fraction (defined as the equivalent concentration of the protein divided by the total ion concentration) is only about 0.11 in 20 mM sodium acetate, making any electrostatic contribution to transport in solution unlikely. Another possibility is that transport is dominated by surface or homogeneous diffusion. This could also explain the high $D_{e,app}/D_0$-values. However, surface or homogeneous diffusion would predict smooth profiles,[13–15] quite unlike those observed experimentally in our case. A final possibility is the existence of parallel pore and surface diffusion mechanisms.[24] However, while such mechanism could describe the macroscopically observed concentration dependence and magnitude of the $D_{e,app}/D_0$ ratio, it would predict concentration profiles exhibiting a sharp front followed by a smooth profile, exactly the opposite of what we see experimentally.

A new model is thus proposed to describe the experimental behavior based on the following hypotheses:

(1) The protein is first weakly partitioned into the pores and then binds strongly on the surface. The strongly bound and weakly partitioned amounts are given by q_a and q_p, respectively, as determined from the adsorption isotherm;

(2) Transport occurs by diffusion with a driving force given by the gradient in q_p. The strongly bound protein is assumed to be immobile; and

(3) The effective diffusion coefficient in the pores is constant and is expected to be similar to that determined from the pulse response experiments under nonbinding conditions.

A pictorial representation of the conceptual model is shown in Figure 7. The solid lines represent the negatively charged agarose matrix. Gray circles represent the protein molecules strongly bound to the agarose backbone, whereas open circles represent protein molecules favorably partitioned in a diffuse electrical double-layer within the liquid-filled pore space. The former molecules, present in concentration q_a, are considered to be immobile, whereas the latter ones, present in concentration q_p, are assumed to possess diffusional mobility of a magnitude similar to that observed for nonbinding conditions. The postulated existence of two families of protein molecules is qualitatively consistent with the shape of the isotherms. As seen from the results in Table 2,

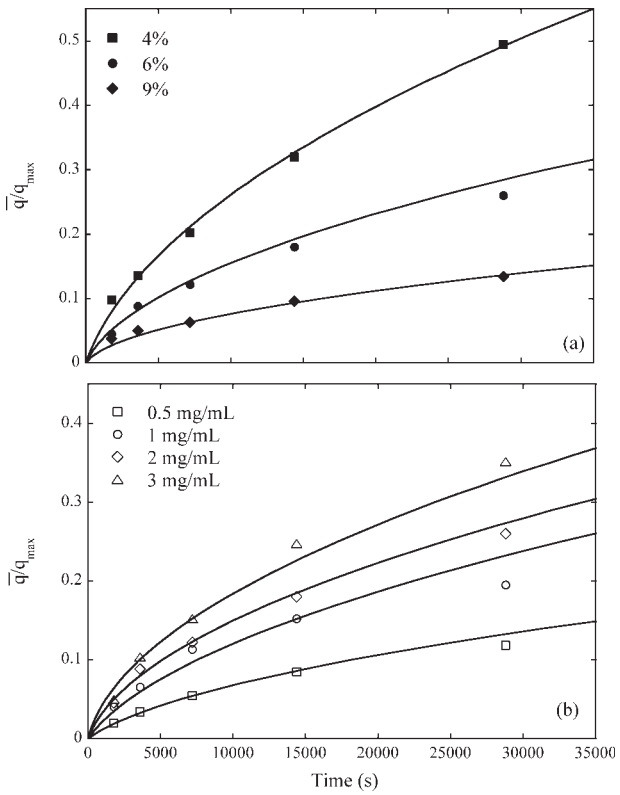

Figure 4. Uptake curves for myoglobin obtained from the microscopic adsorption experiments in gels with different agarose contents.

$\bar{q}$ represents the average protein concentration over a 0.1 cm length. Lines are based on the shrinking core model Eq. 3 with apparent effective diffusivities from Table 3. (a) Effect of agarose content at 2 mg/cm^3 protein concentration. (b) Effect of protein concentration for 6% agarose gel. The 3 mg/cm^3 data are from Schirmer and Carta.[17]

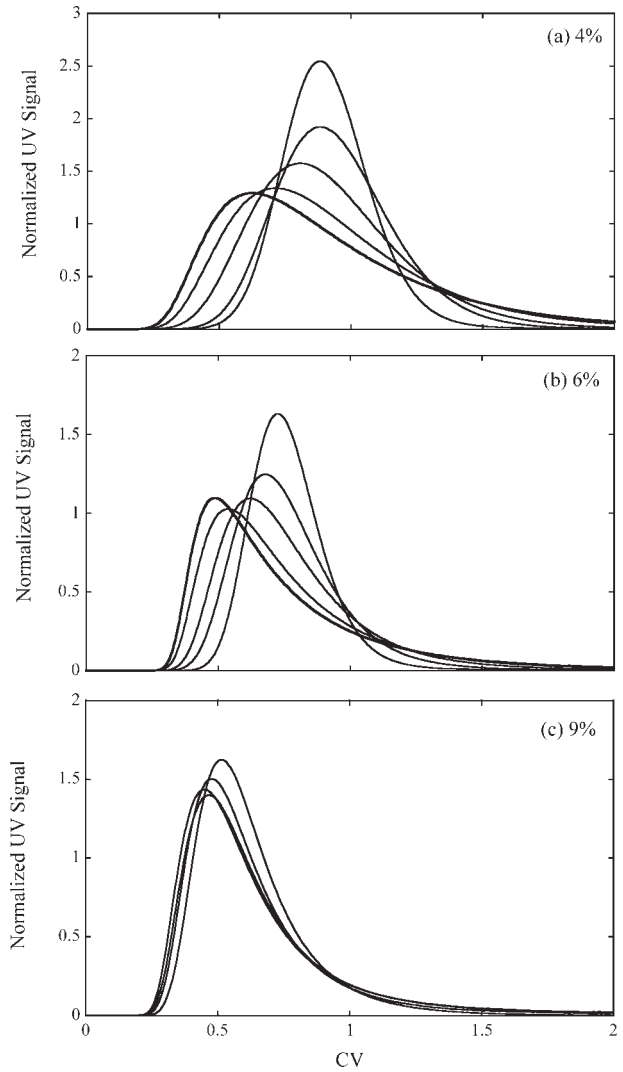

Figure 5. Chromatographic peaks of myoglobin for non-retained conditions for gels with different agarose contents in 5 mm diameter columns.

Flow rates were 0.10, 0.25, 0.50, 1.0, and 1.5 cm^3/min for (a) and (b) and 0.10, 0.15, 0.20, and 0.25 cm^3/min for (c).

$q_{a,m}$, representing the monolayer capacity for the strongly bound protein molecules, varies approximately in proportion to the agarose content. In fact, if this capacity is expressed per unit mass of agarose, we obtain a value of 2.1 ± 0.1 g/g of agarose as an average for the three materials. K_a is also large for all three, which would be expected for strongly favorable binding of the protein on the charged agarose fibers. On the other hand, $q_{p,m}$, representing the maximum concentration of protein partitioned in the fluid-filled pore space also increases with agarose content, which, in turn, is accompanied by a higher charge density, although the K_p values are much smaller. We interpret this result as suggesting q_p actually corresponds to protein that is partitioned in the pores in the region of overlapping electrical potentials.

Further evidence that the protein is likely to exist in two forms within the stationary phase is obtained by considering

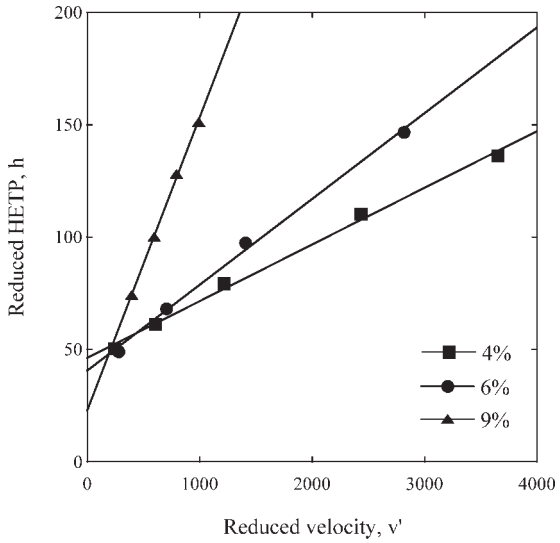

Figure 6. Reduced HETP based on the moment method for gels with different agarose contents.

the reversibility of the adsorption process in response to changes in salt concentration. To test this behavior, 6% agarose particles equilibrated with 2 mg/cm^3 myoglobin were exposed to a solution containing 500 mM NaCl at the same pH. The amount desorbed after 8 h was approximately 20% of the total, which is consistent with the $q_{p,m}$-value in Table 2. We surmise that adding salt removes the protein held in the liquid-filled pore space as a result of highly compressed electrical double layers, without affecting the protein molecules strongly bound to the charged agarose matrix. Interestingly, most of the protein bound, including the strongly held component, could be removed by increasing the pH above the protein pI value.

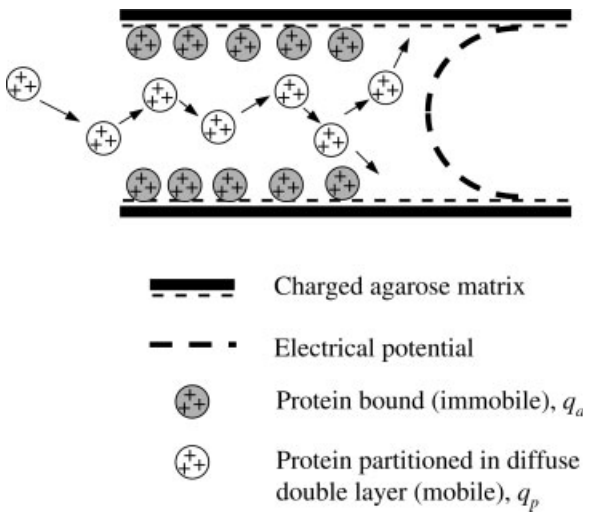

Figure 7. Pictorial representation of the partitioning model.

The concentration gradient of protein partitioned in the pore liquid, ∇q_p, is the driving force for mass transfer.

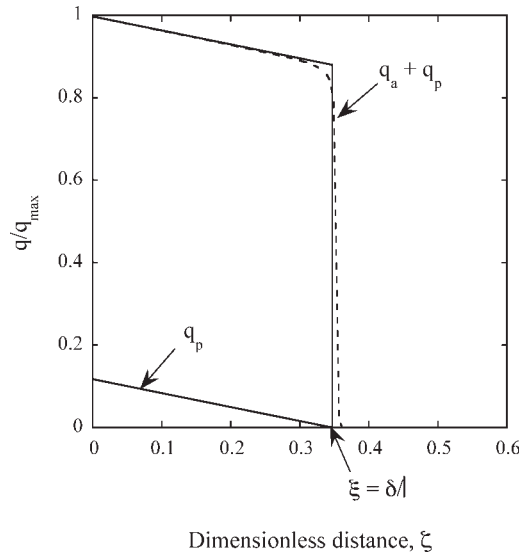

Figure 8. Concentration profiles for the partitioning model, Eqs. 7–9 at dimensionless time $tD_{e,app}/\ell^2 = 0.5$ and $Bi = 180$.

The dashed line is based on the numerical solution of Eq. 4. Equilibrium parameters used are those for 6% agarose in Table 2.

The following equations and boundary conditions are derived based on the hypotheses mentioned earlier:

$$\frac{\partial q_a}{\partial t} + \frac{\partial q_p}{\partial t} = D_{e,app}\nabla^2 q_p \tag{4}$$

$$z = 0: \quad D_{e,app}\nabla q_p = k_f(C_0 - C_s), \qquad C_s = \frac{q_{p,s}}{K_p(q_{p,m} - q_{p,s})} \tag{4a}$$

$$z = \ell: \quad \nabla q_p = 0 \tag{4b}$$

where C_s and $q_{p,s}$ are the interfacial values of C and q_p, respectively. Numerical integration is required in general to solve these equations. However, if $K_a C \gg 1$, the relationship between q_a and C is essentially rectangular ($q_a \sim q_{a,m}$) and a semi-analytical solution can be obtained as follows. With reference to Figure 8 for adsorption in a slab, this limiting case yields a profile that consists of a linear portion followed by sharp drop. Assuming pseudo steady state, the position of the front δ must satisfy the following material balance:

$$\frac{dM}{dt} = \frac{d}{dt}\left(q_{a,m}\delta + \frac{1}{2}q_{p,s}\delta\right) = \frac{D_{e,app}q_{p,s}}{\delta} \tag{5}$$

where M is the total amount of protein in the gel per unit cross section. The surface concentration $q_{p,s}$ is obtained from Eq. 4a. Accordingly,

$$\frac{D_{e,app}q_{p,s}}{\delta} = k_f\left[C_0 - \frac{q_{p,s}}{K_p(q_{p,m} - q_{p,s})}\right] \tag{6}$$

or:

$$q_{p,s} = \frac{1}{2}\left\{\left(q_{p,m} + \frac{1 + K_pC_0}{K_p}Bi\xi\right) - \left[\left(q_{p,m} + \frac{1 + K_pC_0}{K_p}Bi\xi\right)^2 - 4q_{p,m}C_0Bi\xi\right]^{0.5}\right\} \tag{7}$$

where $\xi = \delta/\ell$. The derivative of this equation is given by:

$$\frac{dq_{p,s}}{d\xi} = \frac{Bi}{2}\left\{\frac{1 + K_pC_0}{K_p} - \frac{\frac{1+K_pC_0}{K_p}\left(q_{p,m} + \frac{1+K_pC_0}{K_p}Bi\xi\right) - 2C_0q_{p,m}}{\left[\left(q_{p,m} + \frac{1+K_pC_0}{K_p}Bi\xi\right)^2 - 4C_0q_{p,m}Bi\xi\right]^{0.5}}\right\} \tag{8}$$

Finally, combining Eqs. 5 and 7 yields:

$$\frac{tD_{e,app}}{\ell^2} = \int_0^\xi \left[\frac{q_{a,m}}{q_{p,s}}\zeta + \frac{\zeta}{2} + \frac{1}{2}\frac{\zeta^2}{q_{p,s}}\frac{dq_{p,s}}{d\zeta}\right]d\zeta \tag{9}$$

where $\zeta = z/\ell$ is the integration variable. This equation is the counterpart of Eq. 3 for the new model.

The final result is obtained by numerical integration of Eq. 9. Two special cases, however, yield analytical integrals. The first is when the relationship between q_p and C is linear with slope $K = q_{p,m}K_p$, which yields the solution:

$$\frac{tD_{e,app}}{\ell^2} = \frac{1}{2}\frac{q_{a,m}}{KC_0}\left(\xi^2 + \frac{K}{Bi}\xi\right) + \frac{1}{4}\xi\left(\xi + \frac{2K}{Bi}\right) - \frac{1}{2}\left(\frac{K}{Bi}\right)\ln\left(1 + \frac{Bi}{K}\xi\right) \tag{10}$$

The second case is when the external resistance is neglected, which yields the solution:

$$\frac{tD_{e,app}}{\ell^2} = \left(\frac{q_{a,m}}{2} + \frac{1}{4}\frac{q_{p,m}K_pC_0}{1 + K_pC_0}\right)\xi^2 \tag{11}$$

As an example, Figure 8 compares the profile calculated from Eq. 8 with that obtained directly from the numerical solution of Eq. 4. The latter was obtained by finite differences. For these conditions, there is little difference between the two solutions as the relationship between q_a and C is nearly rectangular.

Comparisons of the new partitioning model with the experimental data for myoglobin adsorption are shown in Figure 9 for the batch uptake rates and in Figures 10 and 11 for the microscopically observed concentration profiles. The fit of the microscopically derived uptake curves, $\overline{q}/q_{max}$ vs. time is not shown explicitly, but was essentially indistinguishable from that based on the shrinking core model depicted in Figure 4. For the batch case, equations analogous to Eq. 4 were written in spherical coordinates and solved numerically taking into account the experimental particle size distribution of each agarose sample together with the material balance for bulk liquid. The particle balances were discretized by finite differences and the global system of ordinary differential

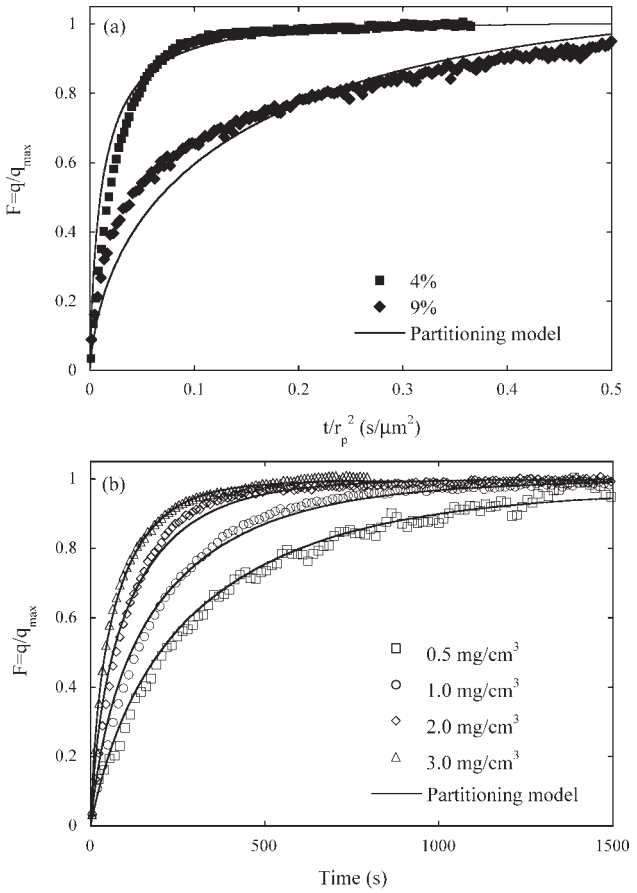

Figure 9. Comparison of experimental and calculated batch uptake curves based on the partitioning model with parameters in Table 3.

(a) Effect of agarose content at 2 mg/cm^3 protein concentration. (b) Effect of protein concentration with 6% agarose gel. The 6% data are from Schirmer and Carta.[17]

equations for each particle size in the distribution solved with Gear's method using IMSL subroutine DIVPAG.

The apparent effective pore diffusivity values obtained from the partitioning model are summarized in Table 3. As seen in Figures 9–11, the model matches both the overall uptake rates quantitatively as well as the concentration profiles in an approximate manner. Most importantly, the corresponding apparent effective diffusivity values are in good agreement with the values obtained from the pulse response experiments under nonbinding conditions. As a result, the D_e/D_0 ratio is much less than unity as expected for ordinary diffusion in the agarose pore matrix. The difference is that the increased protein concentration in the pores under binding conditions enhances the overall rate of mass transfer. As is evident from Figures 10 and 11, the experimental profiles are not as sharp as those predicted by our simple model. A possible explanation is that there is also a kinetic resistance to binding for the strongly adsorbed fraction of the total adsorbed protein. Such resistance was not included in the model. Its incorporation could provide a better fit of the profiles, but, without additional experimental data or independent information, would require the simultaneous fit of multiple kinetic parameters.

Discussion

Two critical issues regarding the physical interpretation of the results of this work need to be addressed. One is the magnitude of the experimentally determined effective diffusivities. The other is the reason for the assumed favorable partitioning of the protein in the pores. With regards to the first issue, the ratio of effective pore diffusivity and free solution diffusivity can be expressed as[20]:

$$\frac{D_e}{D_0} = \frac{\psi_p \varepsilon_p}{\tau_p} \tag{12}$$

where ψ_p is the hindrance factor, ε_p is the porosity, and τ_p is the tortuosity factor of the porous network. The hindrance parameter depends on the ratio of solute and pore radii

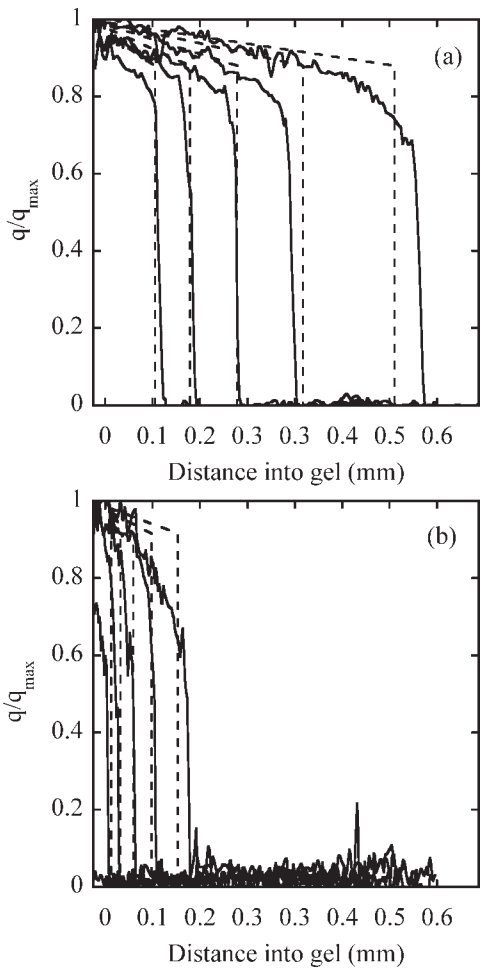

Figure 10. Comparison of experimental (solid lines) and calculated (dashed lines) concentration profiles with 2 mg/cm^3 protein concentration based on the partitioning model with parameters in Table 3 for gels with different agarose content.

Profiles are shown at 30, 60, 120, 240, and 480 min. (a) 4% agarose and (b) 9% agarose.

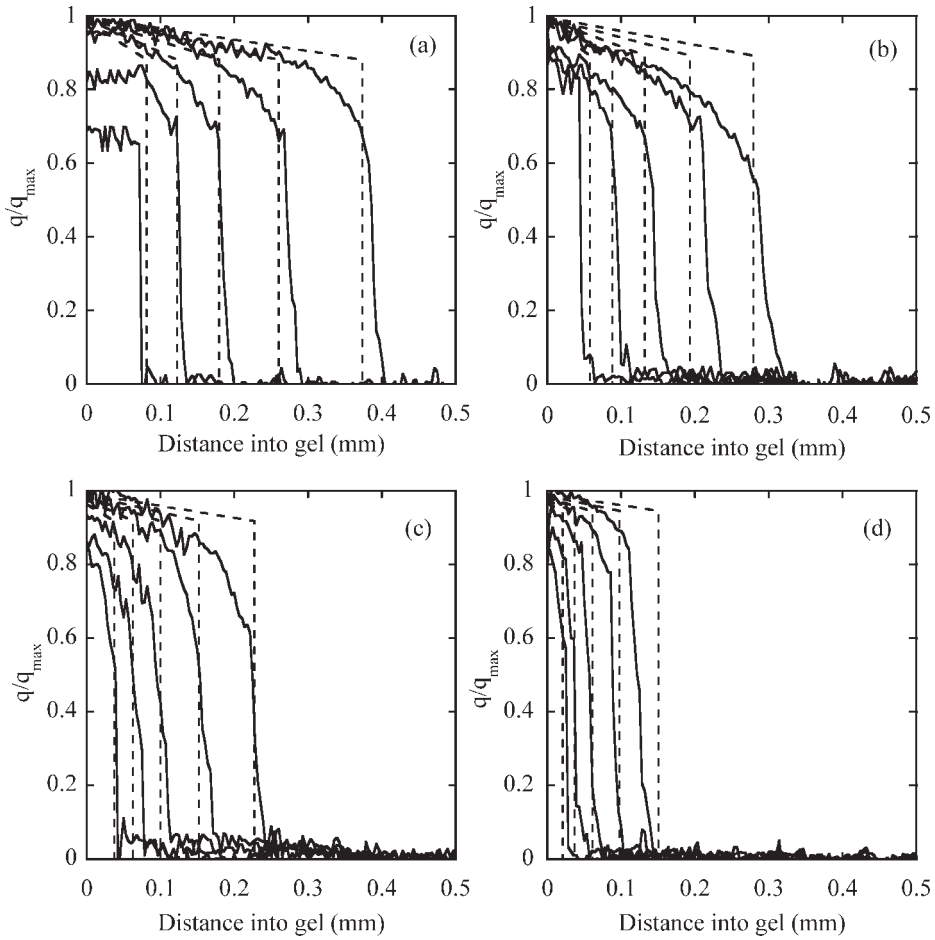

Figure 11. Comparison of experimental (solid lines) and calculated (dashed lines) concentration profiles for 6% agarose gels based on the partitioning model with parameters in Table 3 at different protein concentrations.

Profiles are shown at 30, 60, 120, 240, and 480 min. (a) 3.0, (b) 2.0, (c) 1.0, and (d) 0.5 mg/cm^3. The experimental profiles are from Schirmer and Carta.[17]

($\lambda_m = r_m/r_{pore}$) and can be estimated from the following equations[20,25,26]:

$$\psi_p = \left(1 + \frac{9}{8}\lambda_m \ln \lambda_m - 1.539\lambda_m\right) \text{ for } \lambda_m < 0.2 \qquad (13a)$$

$$\psi_p = 0.865(1-\lambda_m)^2\left(1 - 2.1044\lambda_m + 2.089\lambda_m^3 - 0.984\lambda_m^5\right) \text{ for } \lambda_m > 0.2 \qquad (13b)$$

ε_p is available experimentally for each matrix (see Table 1). Finally, τ_p can be estimated from the equation[20,27]:

$$\tau_p = \frac{(2-\varepsilon_p)^2}{\varepsilon_p} \qquad (14)$$

A comparison of these estimates with the experimentally determined D_e/D_0-values is given in Figure 12, which shows a plot of the ratio $\tau_p D_e/\varepsilon_p D_0$ vs. λ_m. The latter was based on $r_m = 1.9$ nm, obtained from the free solution diffusivity of myoglobin ($D_0 = 1.1 \times 10^{-6}$ cm^2/s),[21] and on the average

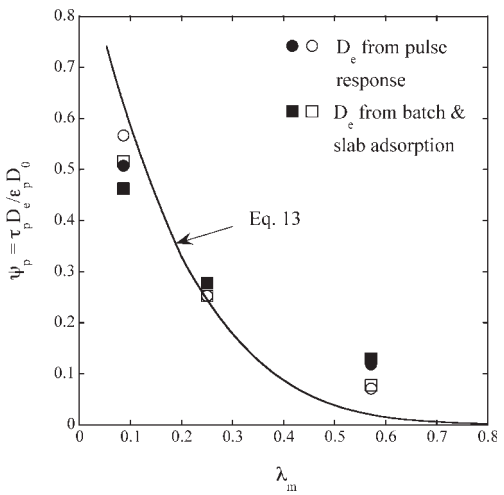

Figure 12. Comparison of experimental and predicted hindrance factors.

Filled symbols are for τ_p estimated from Eq. 14. Open symbols are based on $\tau_p = 1.5$.

pore radius obtained by iSEC for the three different agarose matrices. As the estimation of τ_p based on Eq. 14 is relatively uncertain, the figure also shows the $\tau_p D_e/\varepsilon_p D_0$-ratios calculated with a typical value of $\tau_p = 1.5$. As seen in this figure, the agreement is quite reasonable indicating that the apparent effective diffusivities determined from the pulse response experiments and from the partitioning model fit of the batch and slab adsorption data are consistent with hindered diffusion in the agarose pore network.

With regards to protein partitioning in the pores at low ionic strength, approximate theories are available for spherical colloids in idealized cylindrical pores.[28,29] Accordingly, partitioning is affected by interactions of the charged colloid with the electrical double layer surrounding the pore wall and can be favorable, for example, when the colloid and surface charges are opposite. Although an exact prediction is beyond the scope of this work, it is well established that the possibility of favorable partitioning depends on the thickness of the electrical double layer, which scales with the Debye length[30]:

$$\lambda_D = \sqrt{\frac{\varepsilon_r \varepsilon_0 RT}{2F^2 I}} \tag{15}$$

For our conditions at 20 mM ionic strength $\lambda_D \sim 2.2$ nm. Thus, as the diffuse double layer extends well beyond the Debye length, especially in spherical or cylindrical pores,[31] it is apparent that the electrical potentials overlap in the small pores of our matrices, supporting the underlying assumption of favorable partitioning of the positively charged myoglobin. Increasing I to 520 mM, as in our pulse response experiments, reduces λ_D to about 0.43 nm, thereby making the electrical potential in the bulk of the pore essentially zero, thus largely suppressing favorable partitioning of the protein the pore liquid. From a physical viewpoint, the q_p in our model corresponds to the protein partitioned in the pores. Its magnitude varies between 13.8 and 36.6 mg/cm^3, averaged over the particle volume for agarose contents between 4 and 9%. As seen in Table 1, the higher agarose content is accompanied by a higher charge density which could explain the greater values of q_p obtained for the higher agarose content as a result of the more favorable partitioning of the protein associated with the stronger electrical potential field within the liquid-field pore space.

Conclusions

Myoglobin adsorption and transport in negatively charged agarose gels complies consistently with a mechanism involving partitioning of the protein in the pore liquid followed by strong binding on the surface. As a result, microscopically determined concentration profiles in the gel consist of a nearly linear decline followed by a sharp front. A new model has been developed to describe this behavior. The model successfully predicts the experimental trends with effective pore diffusivities that are in agreement with those determined from pulse response experiments under nonbinding conditions, indicating that the basic nature of diffusive transport is the same in both cases. The main difference is partitioning of the protein in the pores, which is favorable at low ionic strength giving a greater driving force and a faster rate of mass transfer under adsorbing conditions.

Acknowledgments

This work was supported by NSF Grants No. CTS-0414143 and CBET-0729857.

Notation

Bi = Biot number ($=k_f\ell/D_{e,app}$)
C = concentration in the fluid phase, mg/cm^3
C_0 = initial concentration in the fluid phase, mg/cm^3
CV = number of column volumes
$\bar{d}_p$ = average particle diameter, cm
D_0 = free solution diffusivity, cm^2/s
D_e = effective pore diffusivity, cm^2/s
F = Faradays constant
h = reduced height equivalent to theoretical plate ($=\text{HETP}/\bar{d}_p$)
I = ionic strength
K = Langmuir isotherm parameter, Eq. 2
k_f = external film mass transfer coefficient, cm/s
ℓ = length of slab, cm
M_r = protein molecular mass, kDa
q = protein concentration in gel, mg/cm^3
$\bar{q}$ = protein concentration in gel average over length, mg/cm^3
q_m = Langmuir isotherm adsorption capacity, mg/cm^3
q_{max} = maximum total adsorbed concentration, mg/cm^3
$\bar{r}_p$ = average particle radius, cm
$\bar{r}_{pore}$ = average pore radius, nm
r_m = protein radius, nm
Sh = Sherwood number ($= k_f\bar{d}_p/D_0$)
t = time, s
v = interstitial velocity, cm/s
v' = reduced velocity ($=v\bar{d}_p/D_0$)
z = axial coordinate, cm

Greek letters

δ = position of adsorption front, cm
ε = extraparticle porosity
ε_p = intraparticle porosity
λ_D = Debye length
λ_m = ratio of protein and pore radii
τ_p = tortuosity factor
ξ = dimensionless position of adsorption front ($=\delta/\ell$)
ζ = dimensionless axial coordinate ($=z/\ell$)
ψ_p = diffusional hindrance parameter, Eq. 13

Literature Cited

1. Guiochon G, Felinger A, Shirazi DG, Katti AM. *Fundamentals of Preparative and Nonlinear Chromatography*, 2nd edition. New York: Elsevier Academic Press, 2006.
2. Hahn R, Tscheliessnig A, Zöchling A, Jungbauer A. Shallow bed adsorption: theoretical background and applications. *Chem Eng Technol*. 2005;28:1241–1251.
3. Carta G, Ubiera AR, Pabst TM. Protein mass transfer kinetics in ion exchange media: measurements and interpretations. *Chem Eng Technol*. 2005;28:1252–1264.
4. Ljunglöf A, Hjorth R. Confocal microscopy as a tool for studying protein adsorption to chromatographic matrices. *J. Chromatogr A*. 1996;743:75–83.
5. Linden T, Ljunglöf A, Hagel L, Kula MR, Thömmes J. Visualizing patterns of protein uptake to porous media using confocal scanning laser microscopy. *Sep Sci Technol*. 2002;37:1–32.
6. Hubbuch J, Linden T, Knieps E, Thömmes J, Kula MR. Dynamics of protein uptake within the adsorbent particle during packed bed chromatography. *Biotechnol Bioeng*. 2002;80:359–368.
7. Hubbuch J, Linden T, Knieps E, Ljunglöf A, Thömmes J, Kula MR. Mechanism and kinetics of protein transport in chromatographic media studied by confocal laser scanning microscopy. I. The

interplay of sorbent structure and fluid phase conditions. *J Chromatogr A*. 2003;1021:93–104.
8. Dziennik SR, Belcher EB, Barker GA, DeBergalis MJ, Fernandez SE, Lenhoff AM. From the cover: nondiffusive mechanisms enhance protein uptake rates in ion exchange particles. *Proc Nat Acad Sci USA*. 2003;100:420–425.
9. Yang K, Shi Q-H, Sun Y. Modeling and simulation of protein uptake in cation exchanger visualized by confocal laser scanning microscopy. *J Chromatogr A*. 2006;1136:19–28.
10. Harinarayan C, Mueller J, Ljunglöf A, Farhner R, van Alstine J, van Reis R. An exclusion mechanism in ion exchange chromatography. *Biotechnol Bioeng*. 2006;95:775–787.
11. Stone MC, Carta G. Patterns of protein adsorption in chromatographic particles visualized by optical microscopy. *J Chromatogr A*. 2007;1160:206–214.
12. Bankston TE, Stone MC, Carta G. Theory and applications of refractive index based optical microscopy to measure protein mass transfer in spherical adsorbent particles. *J Chromatogr A*. 2008;1188:242–254.
13. Lewus RK, Carta G. Protein diffusion in charged polyacrylamide gels: visualization and analysis. *J Chromatogr A*. 1999;865:155–168.
14. Lewus RK, Carta G. Protein transport in constrained anionic hydrogels: diffusion and boundary-layer mass transfer. *Ind Eng Chem Res*. 2001;40:1548–1558.
15. Russell SM, Belcher EB, Carta G. Protein partitioning and transport in supported cationic acrylamide-based hydrogels. *AIChE J*. 2003; 49:1168–1177.
16. Teske CA, Schroeder M, Simon R, Hubbuch J. Protein-labeling effects in confocal laser scanning microscopy. *J Phys Chem B*. 2005; 109:13811–13817.
17. Schirmer EB, Carta G. Protein adsorption in charged agarose gels studied by light microscopy. *AIChE J*. 2007;53:1472–1482.
18. Do DD. *Adsorption Analysis: Equilibria and Kinetics*. London: Imperial College Press, 1998.
19. Hagel L, Ostberg M, Andersson T. Apparent pore size distributions of chromatography media. *J Chromatogr A*. 1996;743:33–42.
20. LeVan MD, Carta G. Adsorption and ion exchange. In: Perry RH, Green DW, editor. *Perry's Chemical Engineers' Handbook*, 8th edition. New York: McGraw-Hill, 2007: Section 16.
21. Tyn MY, Gusek TW. Prediction of diffusion-coefficients of proteins. *Biotechnol Bioeng*. 1990;35:327–338.
22. Stone MC, Carta G. Protein adsorption and transport in agarose and dextran-grafted agarose media for ion exchange chromatography. *J Chromatogr A*. 2007;1146:202–215.
23. Deen WM, Hindered transport of large molecules in liquid-filled pores. *AIChE J*. 1987;33:1409–1425.
24. Yoshida H, Yoshikawa M, Kataoka T. Parallel transport of BSA by surface and pore diffusion in strongly basic chitosan. *AIChE J*. 1994;40:2034–2044.
25. Brenner H, Gaydos LJ. The constrained Brownian movement of spherical particles in cylindrical pores of comparable radius: models of the diffusive and convective transport of solute molecules in membranes and porous media. *J Coll Int Sci*. 1977;58:312–356.
26. Anderson JL, Quinn JA. Restricted transport in small pores: a model for steric exclusion and hindered particle motion. *Biophys J*. 1974; 14:130–150.
27. Mackie JS, Meares P. The diffusion of electrolytes in a cation-exchange resin membrane. I. Theoretical. *Proc R Soc London*. 1955; 232:498–509.
28. Smith FG, Deen WM. Electrostatic double-layer interactions for spherical colloids in cylindrical pores. *J Coll Int Sci*. 1980;78:444–465.
29. Smith FG, Deen WM. Electrostatic effects on the partitioning of spherical colloids between dilute bulk solution and cylindrical pores. *J Coll Int Sci*. 1983;91:571–590.
30. Probstein RF. *Physicochemical Hydrodynamics: An Introduction*, 2nd edition. New York: Wiley, 1994.
31. Yang Y, Waltz J, Pintauro P. Curvature effects on electric double layer forces, Part 1: Comparisons with parallel plate geometry. *J Chem Soc Farday Trans*. 1995;91:2827–2836.

Manuscript received Jan. 19, 2008, and revision received Aug. 1, 2008.